Peptaibiotic-inspired antimicrobials based on human cathelicidin

John S. Albin[1,2,3], Dimuthu A. Vithanage[2,3], and Bradley L. Pentelute[1,4-6*]

[1]Department of Chemistry, Massachusetts Institute of Technology, Cambridge, MA, 02139, USA

[2]Division of Infectious Diseases, Massachusetts General Hospital, Boston, MA, 02114, USA

[3]Harvard Medical School, Boston, MA, 02115, USA

[4]The Koch Institute for Integrative Cancer Research, Massachusetts Institute of Technology, Cambridge, MA 02142, USA

[5]Center for Environmental Health Sciences, Massachusetts Institute of Technology, Cambridge, MA 02139, USA

[6]Broad Institute of MIT and Harvard, Cambridge, MA 02142, USA

*Correspondence: jalbin@mgh.harvard.edu

Summary: Mammalian cell toxicity of human host defense peptides (HDPs) is a key factor limiting the development of new antibiotic classes based on these natural product templates. In recent work, we have reported both residues in the human cathelicidin LL-37 that reduce its toxicity and strategies for enhancing the potency of short derivatives of LL-37 through mimicry of the LL-37 N-terminus. Here we describe structure-activity relationship studies of one such short derivative, FF-14, in which structure and ultimately separation of hemolytic and antimicrobial functions are supported via the mimicry of Aib-rich peptaibiotic natural products.

Keywords: LL-37, cathelicidin, antimicrobial peptide, host defense peptide, Pseudomonas, antibiotic, peptide

Introduction

Antimicrobial resistance is a growing source of global morbidity and mortality, accounting for more than 1 million deaths per year in recent years with the potential to become the single largest cause of death worldwide in the coming decades[1,3,5]. One strategy to counteract the growing threat posed by antimicrobial resistance is to mine and develop the natural product host defense peptides, which despite their potential benefits have yet to reach clinical use[7,9,11,13].

Humans express a variety of structurally diverse host defense peptides (HDPs), including α defensins, β defensins, histatins, neuropeptides, and a number of miscellaneous protein cleavage products that have varying degrees of reported antimicrobial activity against different microbes[2,17,20]. Humans also express a single cathelicidin, initially as a pro-peptide packaged within neutrophil granules, among other sites, which undergoes cleavage to form the active peptide LL-37 in addition to a number of naturally occurring smaller derivatives[4,6,8]. In its active form, LL-37 is an amphipathic helix that is thought to exert its antimicrobial activity through membrane disruption, though we have recently reported results to suggest that its mechanisms of action may be more complex[10,12]. Regardless, the antimicrobial activity of LL-37 is thought to be dependent upon its helical structure[14,15,18].

Many prior reports have described the activities of diverse fragments of LL-37. Among these fragments, one known as KR-12, spanning residues 18-29 of full-length LL-37, is generally regarded as the minimal unit of LL-37 activity[16]. Recently, we have described a derivative based on this minimal unit that improves activity through mimicry of a biphenyl clamp in the LL-37 N-terminus as well as several chemical modifications that further improve upon the native sequence. In related work, we have also identified mutations in full-length LL-37 that act as mediators of mammalian cell toxicity, I24 and L28, which are also found within the FF-14 template at positions I9 and L13.

Toward the goal of defining a short LL-37 derivative that might minimize mammalian cell toxicity while also maintaining or improving upon low-micromolar activity against gram-negative

bacteria, we carried out systematic Ala scanning of the FF-14 template. In contrast with our prior studies with full-length LL-37, which tolerates extensive combinatorial Ala mutations, mutation of many residues in FF-14, including those previously associated with decreased hemolytic activity, resulted in decreased helical structure and associated losses in antimicrobial activity. Taking inspiration from peptaibiotic natural products, which are characterized by extensive use of the α,α-disubstituted noncanonical amino acid aminoisobutyric acid (Aib) to promote structure[19], we then repeated this scan with Aib, finding an estimated three-fold increases in helical content and associated gains in antimicrobial activity. Through additional testing of combinations of spaced Aib residues, we arrived at combinations that improve upon the *in vitro* therapeutic index of LL-37 by approximately 32-fold. Use of Aib and perhaps other noncanonical α,α-disubstituted amino acids is thus a viable strategy for the promotion of structure and function in peptidomimetics based on helical human cathelicidin templates.

Results

Antimicrobial and hemolytic activity correlate in grouped Ala mutants of FF-14

In our prior studies of surface mutants of LL-37, we described LL-37 mutant m4, which is uniquely able to separate the antibacterial and hemolytic activities of LL-37, thus effectively detoxifying this as a lead antimicrobial. To determine whether it would be possible to achieve this same separation of function in the FF-14 template, we made a series of grouped Ala mutants corresponding to those initially described in full-length LL-37. That is, any set of Ala mutations that occur in mutants covering the 14 amino acids of FF-14 were included. As shown in **Figure 1A-B**, activity of these grouped Ala mutants against *E. coli* and *Pseudomonas* was often attenuated, particularly relative to the corresponding control mutant in the context of full-length LL-37. Moreover, whether a mutant retains antimicrobial activity is largely predictive of whether it will be hemolytic in **Figure 1C**. Thus, mutants that retain antimicrobial activity are generally hemolytic, and mutants that lack antimicrobial activity are generally nonhemolytic. This stands in contrast with mutant m4, which as in our prior studies clearly separates hemolytic and antibacterial functions. Mutants used in these studies are shown in **Figure 1D**.

To determine whether these activity patterns might correlate with helical content, we analyzed these mutants by circular dichroism (CD) spectroscopy. Spectra for each mutant are shown in **Supplementary Figure 1A-G**. Helical content as calculated using BeStSel[21] is summarized in **Supplementary Figure 1H**. Although some mutants, particularly FF-14 m4 and FF-14 m4-FF, appear to lose structure, this correlation does not necessarily hold among other mutants such as FF-14 m5 and FF-14 m5-FF, which show appreciable helical content but nevertheless lose both hemolytic and antimicrobial function. **Supplementary Figure 2** shows the data from **Figure 1** in histogram format including error bars. The kinetic curves associated with the endpoint data provided in **Figure 1** are shown in **Supplementary Figures 3-14** (antimicrobial susceptibility testing) and **Supplementary Figures 15-26** (hemolysis assays). A standardized, quantitative presentation of **Figure 1** data is provided in **Supplementary Table 1**.

Antimicrobial and hemolytic activities correlate in single Ala mutants of FF-14

In our prior work on LL-37, we have found that full-length LL-37 tolerates up to at least eight simultaneous Ala mutants out of the 37-mer sequence without losing helical structure (see **Figure 1D**). Based on the results of **Figure 1**, however, it appeared that the FF-14 scaffold, while itself helical, may be less tolerant of alterations. We therefore hypothesized that the scaffold might better tolerate single Ala mutations and proceeded to make a series of single Ala mutants covering the FF-14 sequence.

Antimicrobial susceptibility testing as shown in **Figure 2A-B** demonstrated modest improvement in activity with mutants R8A and D11A, the latter in particular echoing prior similar evaluations in the context of KR-12[22]. The primary losses in activity localized to I9A and L13A, corresponding to the primary mutations responsible for separation of antibacterial and hemolytic activity in full-length LL-37, I24 and L28 – both of which are mutated to Ala as part of the m4 complement of mutations in **Figure 1**. These mutations are also associated with a substantially decreased propensity for self-interaction. Although this loss of self-interaction does not affect the antimicrobial activity of full-length LL-37, it is possible that the shorter FF-14 scaffold may be less stable as a monomer. Overall, there was a strong correlation between antimicrobial and hemolytic potency among the mutants tested in this series (**Figure 2C**). Thus, Ala scanning mutants do not reveal a means by which to separate antimicrobial and hemolytic functions in LL-37. **Supplementary Figure 27** shows the data from **Figure 2** in histogram format including error bars. The kinetic curves associated with the endpoint data provided in **Figure 2** are shown in **Supplementary Figures 28-42** (antimicrobial susceptibility testing) and **Supplementary Figures 43-57** (hemolysis assays). A standardized, quantitative presentation of **Figure 2** data is provided in **Supplementary Table 2**.

Modest correlation between antimicrobial activity and FF-14 Ala mutant helical content

Based on the loss of helical content associated with FF-14 m4 grouped mutants in **Figure 1** and **Supplementary Figure 1**, we hypothesized that helical content might correlate with antimicrobial activity among single Ala mutants. To directly assess this, we again collected CD spectra from each of the single Ala mutants used in **Figure 2**. As shown in **Supplementary Figure 58**, strong or absent helical content is generally associated with strong or weak antimicrobial activity, respectively. For example, the R8A and D11A mutants are strongly helical and more active than wild-type FF-14, while the I9A and L13A mutants are largely disordered and largely inactive. Incorporating the middle of this range, however, shows only a modest correlation among the calculated percent helical content in these mutants in comparison with the log2 of their MIC against *E. coli*. Thus, helical content appears predictive of activity at the extremes, but less so for intermediate values, consistent with prior studies demonstrating the importance of helical structure for LL-37 activity[8,14]. Individual spectra are provided in **Supplementary Figure 59**.

Incorporation of aminoisobutyric acid (Aib) improves FF-14 antimicrobial activity

In the context of full-length LL-37, the combination of I24A and L28A largely recapitulates the separation of function phenotype of the LL-37 m4 mutant. The equivalent positions in FF-14 are I9 and L13, both of which lose both structure and activity when changed to Ala in **Figure 2**. We therefore hypothesized that supporting the helical structure of the underlying peptide with mutations at these and other positions might afford improved antimicrobial activity and, in the case of I9 and L13, separation of hemolytic function, a premise inspired by peptaibiotic natural products in which the frequent occurrence of Aib supports helical structure[19] in addition to prior studies demonstrating the ability of Aib to support peptide helical structure (*e.g.*, [23,25]).

To test this hypothesis, we made a series of mutants corresponding to those in **Figure 2** in which, rather than substituting a given position with Ala, we instead inserted Aib. As shown in

Figure 3A-B, antimicrobial activity with Aib substitution was neutral to improved at all residues relative to Ala. This was particularly true of F2, I5, and I9, where substitution of Aib in place of Ala results in 8-fold improvements in MIC against *E. coli*. Despite this improvement in antimicrobial activity, hemolytic activity was typically neutral to increased with Aib substitution with the exception of D11 (**Figure 4C**). A summary of the mutants used in these studies is shown in **Figure 3D**. **Supplementary Figure 60** shows the data from **Figure 3** in histogram format including error bars. The kinetic curves associated with the endpoint data provided in **Figure 3** are shown in **Supplementary Figures 61-76** (antimicrobial susceptibility testing) and **Supplementary Figures 77-92** (hemolysis assays). A standardized, quantitative presentation of **Figure 3** data is provided in **Supplementary Table 3**.

Aib substitution within the FF-14 scaffold enhances helical content and antimicrobial activity with modest effects on overall therapeutic index

Table 1 summarizes quantitative changes in helical content, antimicrobial activity, hemolytic activity, and the ratio of hemolytic to antimicrobial activity for a matched set of Ala versus Aib substitutions along the length of the FF-14 scaffold. Overall helical content increased an average of three-fold with Aib substitution, which was mirrored by an average three-fold improvement in antimicrobial activity among Aib mutants. Hemolytic activity of Aib mutants typically increased relative to Ala, though to a lesser degree than the increase in antimicrobial activity. The net effect was a more modest increase in the ratio of the hemolytic to antimicrobial activity levels of matched mutants, averaging 1.6-fold with 2-4-fold increases at F2, I5, Q7, and D11. Thus, Aib substitution typically improves helical content and antimicrobial activity with lesser effects on overall therapeutic indices. CD spectra for Aib-substituted mutants are shown in **Supplementary Figure 93.**

Selected Aib double-mutants promote helical structure and improved therapeutic properties

Given the ability of single Aib mutants to promote helical structure, we reasoned that double mutants might yield further improvements. To test this hypothesis, we made a series of four "pseudostapled" mutants in which Aib was substituted at paired *i,i+4* positions along the helical hydrophobic surface at residues 1+5, 2+6, 5+9, and 9+13. Among these, all except for I9B+L13B retained appreciable activity against *E. coli* (**Figure 4A**), with F2B+V6B being the most active. CD spectra of these mutants suggested that F2B+V6B and F1B+I5B retained the most helical content (**Supplementary Figure 94**). To determine whether it would be possible to substitute additional Aib mutations into this structure that might contribute to detoxification of the parent template, we made three additional mutants adding the LL-37 detoxification mutations I9B and/or L13B to the F2B+V6B scaffold. Among these, activity remained equal to that of parent F2B+V6B when adding I9B, but with an increase of two dilutions in the threshold hemolysis level to 50 µM, thus overall yielding a 32-fold improvement in *in vitro* therapeutic index over parent LL-37 (**Figure 4C**). Despite these improvements in *E. coli*, however, the Aib mutants tested generally fared poorly against *Pseudomonas*; whether there are additional changes that may restore activity within this scaffold is as yet undetermined. Thus, a combination of 2-3 Aib residues within the FF-14 scaffold can improve both antimicrobial activity and hemolytic activity compared with the parent residue and with standard Ala mutations.

Supplementary Figure 95 shows the data from **Figure 4** in histogram format. **Supplementary Figures 96-105** (antimicrobial susceptibility testing) and **106-115** (hemolysis) show the kinetic curves associated with the endpoint measures in **Figure 4**. A standardized, quantitative presentation of **Figure 4** data is provided in **Supplementary Table 4**.

Aib-induced helices may not be stable to further modifications

Given the ability of Aib to improve helical content, we next asked whether pairing Aib residues with canonical amino acids elsewhere might yield "pseudostapled" templates that would be stable to changes elsewhere in the sequence. For certain residues, this strategy yields overall improvement. For example, while I9A ablates activity in the FF-14 template (**Figure 2**), activity of this mutant in the context of 2+6 is 25 μM with a neutral Fold Δ (see also **Supplementary Table 5**). For most Ala mutations, however, the overall Fold Δ goes down, driven primarily by decreases in antimicrobial activity. A comparison between the effects of Ala mutations when introduced into 2+6 versus the FF-14 template shows that the Fold Δ generally decreases when mutations are introduced into 2+6, while this same value generally stays neutral or improved when introduced into FF-14 (**Supplementary Table 6**). Rather than allowing isolated substitutions to remain phenotypically isolated, then, it is likely that further sequence changes in the 2+6 template – and perhaps in most templates – would require one to account for the combinatorial effects of multiple mutations.

Supplementary Figure 116 shows the data from **Figure 5** in histogram format. **Supplementary Figures 117-131** (antimicrobial susceptibility testing) and **132-146** (hemolysis) show the kinetic curves associated with the endpoint measures in **Figure 5**.

Discussion

We describe here a systematic mutagenesis effort aimed at promoting structure, activity, and separation of hemolytic and antimicrobial functions of the human cathelicidin-derived scaffold FF-14 through peptaibiotic-inspired modifications. Consistent with prior literature on full-length LL-37[14], we find that helical structure is critical for cathelicidin function, and we demonstrate the ability to support structure in this human HDP-derived scaffold through the incorporation of the α,α-disubstituted noncanonical amino acid Aib. To our knowledge, this is the first attempt to combine the features of a human HDP with this distinct category of natural

products. The principles explored here are likely to be applicable to other human cathelicidin derivatives, and perhaps to other human HDP scaffolds.

Based on a matched dataset of Ala and Aib substitutions along the length of the FF-14 scaffold, Aib incorporation results in an average three-fold increase in helical content, with a similar average fold-increase in antimicrobial activity. Despite these benefits, however, individual changes had limited impacts on hemolytic activity. Through an iterative process of testing combinations of Aib residues, we ultimately arrived at a second generation derivative based on the FF-14 scaffold consisting of three Aib substitutions at residues F2, V6, and I9 in FF-14 numbering (F17, V21, and I24 in LL-37 numbering). Together, these yielded a short cathelicidin-derived candidate with a low single-digit micromolar MIC against *E. coli* and an *in vitro* therapeutic index approximately 32 times greater than that of native LL-37.

In related work, we have recently identified mutations in full-length LL-37 that inhibit LL-37's ability to form oligomeric structures, which is associated with decreased activity against mammalian cell membranes – though not solely responsible. One such example is m4 in **Figure 1**, which achieves a 256-fold improvement in *in vitro* therapeutic index over the LL-37 scaffold in that series of experiments[27,30]. In other work, we have noted truncation mutants of LL-37 that also appear to separate hemolytic and antibacterial activities, likely by eliminating a critical portion of this self-interaction region[32,33]. As has been found previously in other cathelicidin scaffolds, helical structure is critical for peptide activity. Although we have not formally tested this, it is possible that part of the challenge in adapting our detoxification mutations from the 37-mer scaffold to a 14-mer scaffold was that the shorter scaffold was less tolerant of a decreased capacity for oligomerization. Regardless of the exact underlying mechanism, our function data suggest that use of α,α-disubstituted amino acids may be a chemically simpler method to promote structure in these templates than alternatives such as various stapling chemistries. In principle, a single noncanonical amino acid is technically feasible for use in expression systems,

such that biomanufacturing of such peptaibiotic-like derivatives may help to hold down the costs of any downstream therapeutics[34,35].

Despite the success of our work in incorporating at least one detoxifying residue into an FF-14-derived scaffold using a traditional development approach, the combinatorial matrix from this point forward becomes increasingly complicated. In **Figure 5**, we had hypothesized that the 2+6 scaffold would be able to tolerate mutation at various sites without losses in activity. Unlike the FF-14 scaffold where Ala substitutions generally resulted in neutral or improved compound performance, Ala substitutions in 2+6 generally resulted in neutral or worsened compound performance. An optimistic interpretation of these data are that this decrease in the 2+6 scaffold was usually not so great as to cause more than a 2-fold drop in activity. Moreover, the total number of scenarios tested is small, and it is possible that substitutions other than Ala may result in more favorable outcomes. Within the dataset that we have, though, it appears that many individual substitutions into a scaffold such as 2+6 may adversely impact overall compound performance. If that is true, it may become necessary to test a large number of combinations that would be prohibitively time-consuming and expensive under standard approaches. That is, while some modifications such as N-lipidation and C-amidation that we have described previously in the context of FF-14 may be more straightforward to test by traditional means, others than involve sequence changes such as the use of D- amino acids or more noncanonical residues like Aib may necessitate the exploration of massive combinatorial spaces unnavigable by standard approaches.

Anticipating such a scenario, we have recently developed methods for the rapid flow synthesis of combinatorial polyamide libraries, in part for application to problems such as this in which a large combinatorial matrix may need to be tested simultaneously via selection-based drug discovery approaches[28]. Using this system, we can generate chemical libraries of effectively any size up to quintillions of members with the same time and reagent usage required to make a single peptide – for a 14-mer, < 1 hour. Current research is focused on

applying concurrently developed deconvolution methods to building out a broader platform of selection systems. In principle, though, rather than individually making hundreds or thousands or millions, etc., of peptides, it may instead be possible to use saturating mutagenesis to quickly probe for all possible combinations of residues of interest that are consistent with a selectable phenotype.

One such phenotype that immediately becomes apparent is the gradual decrease in activity against *Pseudomonas* over the course of the studies described here, which may be counteracted by selecting for combinations within the 2+6 I9B scaffold that reverse this. Similarly, we use colistin throughout as a model of what an approved, albeit relatively toxic, antibiotic looks like in our system. Although 2+6 I9B is a marked improvement over LL-37, and a tractable candidate for further development, another important area for ongoing improvement is further addressing toxicity. This too may be a good task for combinatorial chemistry given the size of the potential testing matrix involved.

In summary, we report here peptaibiotic-inspired modifications to a human cathelicidin HDP template. The resultant lead antimicrobial, 2+6 I9B, achieves low single-digit micromolar inhibition of *E. coli* consistent with the MICs associated with approved antimicrobials[36] and a therapeutic index approximately 32 times greater than that of native LL-37. 2+6 I9B is thus a candidate for further development of novel agents active against gram-negative bacteria, and the principles of Aib incorporation to support helical structure may be broadly applicable to human cathelicidin and other human HDP templates.

Methods

Peptide synthesis and purification –

Peptide synthesis was completed as previously described on third generation automated flow peptide synthesizers[24,26,29]. Aib residues were coupled as Ala (21 strokes HATU). Following synthesis, peptides were cleaved with Reagent K (82.5% trifluoroacetic acid (TFA), 5% water, 5% phenol, 2.5% ethanedithiol) for 2 hours at room temperature followed by peptide precipitation in ether chilled on dry ice. Following precipitation, precipitated peptide was resuspended in 50% water / 50% acetonitrile with 0.1% TFA, flash frozen in liquid nitrogen, and lyophilized. Peptide purification was carried out on reverse phase columns with a Biotage Selekt flash chromatography system, with subsequent confirmation of the peptide identity and purity by liquid chromatography-mass spectrometry and high performance liquid chromatography.

Circular dichroism spectroscopy –

Peptides were dissolved in water at 0.5 mg/mL. Trifluoroethanol was then added to 20% v/v, and spectra were collected on an Aviv 420 spectrometer at the indicated temperatures in 0.1 cm pathlength cuvettes. Spectra were analyzed for secondary structural content using BeStSel[21].

Antimicrobial susceptibility testing –

Antimicrobial susceptibility testing was completed as per Clinical & Laboratory Standards Institute guidelines with modifications previously described for cationic peptides, including the use of polypropylene plates and unadjusted Mueller Hinton Broth[31]. Protocols were scaled down to either 35 or 50 µL in 384-well plates. After plating, wells were monitored for growth by OD600 over 18 hours at 37 °C in a Tecan Spark plate reader with a Large Humidity Cassette to minimize evaporation.

Hemolysis assays –

Hemolysis assays were completed in 50 µL per well in 384-well plates in a fashion similar to antimicrobial susceptibility testing above. Defibrinated sheep blood (Hardy Diagnostics) was spun at 800 rcf for 10 minutes and washed with PBS to visual clearance. Remaining blood was then resuspended in PBS at 1% v/v. Following the addition of 25 µL of 2x target concentrations of antibiotic dissolved in PBS to 384-well plates, the 1% blood suspension was added for a final concentration of 0.5% v/v. Hemolysis was then monitored kinetically by OD600 in a Tecan Spark plate reader as for antimicrobial susceptibility testing. In addition to this kinetic measure, hemolysis was monitored as an endpoint measurement by the addition of 25 µL of PBS at 18 hours, spinning for 10 minutes at 800 rcf, and then removing 25 µL of supernatant to a new 384-well plate to be read at 414 nm for free hemoglobin.

Acknowledgements

This work has been funded by the National Institute of Allergy and Infectious Diseases (T32 AI007061 and K08 AI166345 to JSA; U19 AI142780 to BLP) and by the Cystic Fibrosis Foundation (ALBIN19F0, ALBIN21Q0, ALBIN22A0-KB to JSA).

Author Contributions

JSA designed and conducted the experiments and wrote the paper. BLP and DTH guided the experiments and wrote the paper.

Declaration of Interests

JSA declares no competing interests.

References

1. The Review on Antimicrobial Resistance (2014). Antimicrobial Resistance: Tackling a Crisis for the Health and Wealth of Nations. 2014.

2. Wang, G., Li, X., and Wang, Z. (2016). APD3: the antimicrobial peptide database as a tool for research and education. Nucleic Acids Res *44*, D1087–D1093. https://doi.org/10.1093/nar/gkv1278.

3. Murray, C.J., Ikuta, K.S., Sharara, F., Swetschinski, L., Robles Aguilar, G., Gray, A., Han, C., Bisignano, C., Rao, P., Wool, E., et al. (2022). Global burden of bacterial antimicrobial resistance in 2019: a systematic analysis. The Lancet *399*, 629–655. https://doi.org/10.1016/S0140-6736(21)02724-0/ATTACHMENT/B227DEB3-FF04-497F-82AC-637D8AB7F679/MMC1.PDF.

4. Sørensen, O.E., Follin, P., Johnsen, A.H., Calafat, J., Sandra Tjabringa, G., Hiemstra, P.S., and Borregaard, N. (2001). Human cathelicidin, hCAP-18, is processed to the antimicrobial peptide LL-37 by extracellular cleavage with proteinase 3. Blood *97*, 3951–3959. https://doi.org/10.1182/BLOOD.V97.12.3951.

5. Naghavi, M., Vollset, S.E., Ikuta, K.S., Swetschinski, L.R., Gray, A.P., Wool, E.E., Robles Aguilar, G., Mestrovic, T., Smith, G., Han, C., et al. (2024). Global burden of bacterial antimicrobial resistance 1990-2021: a systematic analysis with forecasts to 2050. Lancet *404*, 1199–1226. https://doi.org/10.1016/S0140-6736(24)01867-1.

6. Dürr, U.H.N., Sudheendra, U.S., and Ramamoorthy, A. (2006). LL-37, the only human member of the cathelicidin family of antimicrobial peptides. Biochimica et Biophysica Acta (BBA) - Biomembranes *1758*, 1408–1425. https://doi.org/10.1016/J.BBAMEM.2006.03.030.

7. Magana, M., Pushpanathan, M., Santos, A.L., Leanse, L., Fernandez, M., Ioannidis, A., Giulianotti, M.A., Apidianakis, Y., Bradfute, S., Ferguson, A.L., et al. (2020). The value of antimicrobial peptides in the age of resistance. Lancet Infect Dis *20*, e216–e230. https://doi.org/10.1016/S1473-3099(20)30327-3.

8. Turner, J., Cho, Y., Dinh, N.N., Waring, A.J., and Lehrer, R.I. (1998). Activities of LL-37, a cathelin-associated antimicrobial peptide of human neutrophils. Antimicrob Agents Chemother *42*, 2206–2214.

9. Mourtada, R., Herce, H.D., Yin, D.J., Moroco, J.A., Wales, T.E., Engen, J.R., and Walensky, L.D. (2019). Design of stapled antimicrobial peptides that are stable, nontoxic and kill antibiotic-resistant bacteria in mice. Nat Biotechnol *37*, 1186–1197. https://doi.org/10.1038/s41587-019-0222-z.

10. Erriah, P., Puan, S.L., Yahaya, N.M., Wan Ahmad Kamil, W.N.I., Amin Nordin, S., Muhamad, A., and Sabri, S. (2025). Harnessing bacterial antimicrobial peptides: a comprehensive review on properties, mechanisms, applications, and challenges in combating antimicrobial resistance. J Appl Microbiol *136*, 290. https://doi.org/10.1093/JAMBIO/LXAE290.

11. Martin-Loeches, I., Dale, G.E., and Torres, A. (2018). Murepavadin: a new antibiotic class in the pipeline. Expert Rev Anti Infect Ther *16*, 259–268. https://doi.org/10.1080/14787210.2018.1441024.

12. Andersson, D.I., Hughes, D., and Kubicek-Sutherland, J.Z. (2016). Mechanisms and consequences of bacterial resistance to antimicrobial peptides. Drug Resistance Updates *26*, 43–57. https://doi.org/10.1016/J.DRUP.2016.04.002.

13. Srinivas, N., Jetter, P., Ueberbacher, B.J., Werneburg, M., Zerbe, K., Steinmann, J., Van der Meijden, B., Bernardini, F., Lederer, A., Dias, R.L.A., et al. (2010). Peptidomimetic antibiotics target outer-membrane biogenesis in Pseudomonas aeruginosa. Science *327*, 1010–1013. https://doi.org/10.1126/science.1182749.

14. Johansson, J., Gudmundsson, G.H., Rottenberg, M.E., Berndt, K.D., and Agerberth, B. (1998). Conformation-dependent Antibacterial Activity of the Naturally Occurring Human Peptide LL-37. Journal of Biological Chemistry *273*, 3718–3724. https://doi.org/10.1074/JBC.273.6.3718.

15. Wang, G. (2008). Structures of Human Host Defense Cathelicidin LL-37 and Its Smallest Antimicrobial Peptide KR-12 in Lipid Micelles. Journal of Biological Chemistry *283*, 32637–32643. https://doi.org/10.1074/JBC.M805533200.

16. Wang, G. (2008). Structures of human host defense cathelicidin LL-37 and its smallest antimicrobial peptide KR-12 in lipid micelles. Journal of Biological Chemistry *283*, 32637–32643. https://doi.org/10.1074/jbc.M805533200.

17. Hancock, R.E.W., Haney, E.F., and Gill, E.E. (2016). The immunology of host defence peptides: beyond antimicrobial activity. Nat Rev Immunol *16*, 321–334. https://doi.org/10.1038/nri.2016.29.

18. Li, X., Li, Y., Han, H., Miller, D.W., and Wang, G. (2006). Solution structures of human ll-37 fragments and NMR-based identification of a minimal membrane-targeting antimicrobial and anticancer region. J Am Chem Soc *128*, 5776–5785. https://doi.org/10.1021/JA0584875/SUPPL_FILE/JA0584875SI20051222_013003.PDF.

19. Hou, X., Sun, R., Feng, Y., Zhang, R., Zhu, T., Che, Q., Zhang, G., and Li, D. (2022). Peptaibols: Diversity, bioactivity, and biosynthesis. Engineering Microbiology *2*, 100026. https://doi.org/10.1016/J.ENGMIC.2022.100026.

20. Haney, E.F., Straus, S.K., and Hancock, R.E.W. (2019). Reassessing the Host Defense Peptide Landscape. Front Chem *7*, 43. https://doi.org/10.3389/fchem.2019.00043.

21. Micsonai, A., Wien, F., Kernya, L., Lee, Y.H., Goto, Y., Réfrégiers, M., and Kardos, J. (2015). Accurate secondary structure prediction and fold recognition for circular dichroism spectroscopy. Proc Natl Acad Sci U S A *112*, E3095–E3103. https://doi.org/10.1073/PNAS.1500851112/SUPPL_FILE/PNAS.201500851SI.PDF.

22. Gunasekera, S., Muhammad, T., Strömstedt, A.A., Rosengren, K.J., and Göransson, U. (2018). Alanine and Lysine Scans of the LL-37-Derived Peptide Fragment KR-12 Reveal Key Residues for Antimicrobial Activity. Chembiochem *19*, 931–939. https://doi.org/10.1002/CBIC.201700599.

23. Vasudev, P.G., Chatterjee, S., Narayanaswamy, S., and Padmanabhan, B. (2011). Structural chemistry of peptides containing backbone expanded amino acid residues: Conformational features of β, γ, and hybrid peptides. Chem Rev *111*, 657–687. https://doi.org/10.1021/CR100100X/SUPPL_FILE/CR100100X_SI_002.PDF.

24. Albin, J.S., and Pentelute, B.L. (2020). Efficient flow synthesis of human antimicrobial peptides. Aust J Chem *73*, 380–388. https://doi.org/10.1071/CH20043.

25. Karle, I.L., and Balaram, P. (1990). Structural Characteristics of α-Helical Peptide Molecules Containing Aib Residues. Biochemistry *29*, 6747–6756. https://doi.org/10.1021/BI00481A001/ASSET/BI00481A001.FP.PNG_V03.

26. Hartrampf, N., Saebi, A., Poskus, M., Gates, Z.P., Callahan, A.J., Cowfer, A.E., Hanna, S., Antilla, S., Schissel, C.K., Quartararo, A.J., et al. (2020). Synthesis of proteins by automated flow chemistry. Science (1979) *368*, 980–987. https://doi.org/10.1126/science.abb2491.

27. Sancho-Vaello, E., Gil-Carton, D., François, P., Bonetti, E.J., Kreir, M., Pothula, K.R., Kleinekathöfer, U., and Zeth, K. (2020). The structure of the antimicrobial human cathelicidin LL-37 shows oligomerization and channel formation in the presence of membrane mimics. Scientific Reports 2020 10:1 *10*, 1–16. https://doi.org/10.1038/s41598-020-74401-5.

28. Albin, J.S., Lee, G.Y., Johnson, C., Vithanage, D.A., Vuong, W., and Pentelute, B.L. (2025). Rapid generation of hypervariable chemical libraries. Chem *0*, 102501. https://doi.org/10.1016/J.CHEMPR.2025.102501.

29. Mijalis, A.J., Thomas, D.A., Simon, M.D., Adamo, A., Beaumont, R., Jensen, K.F., and Pentelute, B.L. (2017). A fully automated flow-based approach for accelerated peptide synthesis. Nat Chem Biol *13*, 464–466. https://doi.org/10.1038/nchembio.2318.

30. Sancho-Vaello, E., François, P., Bonetti, E.J., Lilie, H., Finger, S., Gil-Ortiz, F., Gil-Carton, D., and Zeth, K. (2017). Structural remodeling and oligomerization of human cathelicidin on membranes suggest fibril-like structures as active species. Sci Rep *7*. https://doi.org/10.1038/S41598-017-14206-1.

31. Wiegand, I., Hilpert, K., and Hancock, R.E.W. (2008). Agar and broth dilution methods to determine the minimal inhibitory concentration (MIC) of antimicrobial substances. Nat Protoc *3*, 163–175. https://doi.org/10.1038/nprot.2007.521.

32. Burton, M.F., and Steel, P.G. (2009). The chemistry and biology of LL-37. Preprint at The Royal Society of Chemistry, https://doi.org/10.1039/b912533g https://doi.org/10.1039/b912533g.

33. Braff, M.H., Hawkins, M.A., Di Nardo, A., Lopez-Garcia, B., Howell, M.D., Wong, C., Lin, K., Streib, J.E., Dorschner, R., Leung, D.Y.M., et al. (2005). Structure-function relationships among human cathelicidin peptides: dissociation of antimicrobial properties from host immunostimulatory activities. J Immunol *174*, 4271–4278. https://doi.org/10.4049/jimmunol.174.7.4271.

34. Niu, W., and Guo, J. (2024). Cellular Site-Specific Incorporation of Noncanonical Amino Acids in Synthetic Biology. Chem Rev.

https://doi.org/10.1021/ACS.CHEMREV.3C00938/ASSET/IMAGES/MEDIUM/CR3C00938_0024.GIF
.

35. Biava, H.D. (2020). Tackling Achilles' Heel in Synthetic Biology: Pairing Intracellular Synthesis of Noncanonical Amino Acids with Genetic-Code Expansion to Foster Biotechnological Applications. Chembiochem *21*, 1265–1273. https://doi.org/10.1002/CBIC.201900756.

36. CLSI eClipse Ultimate Access - Powered by Edaptive Technologies https://em100.edaptivedocs.net/Login.aspx?ru=1&emsg=275.

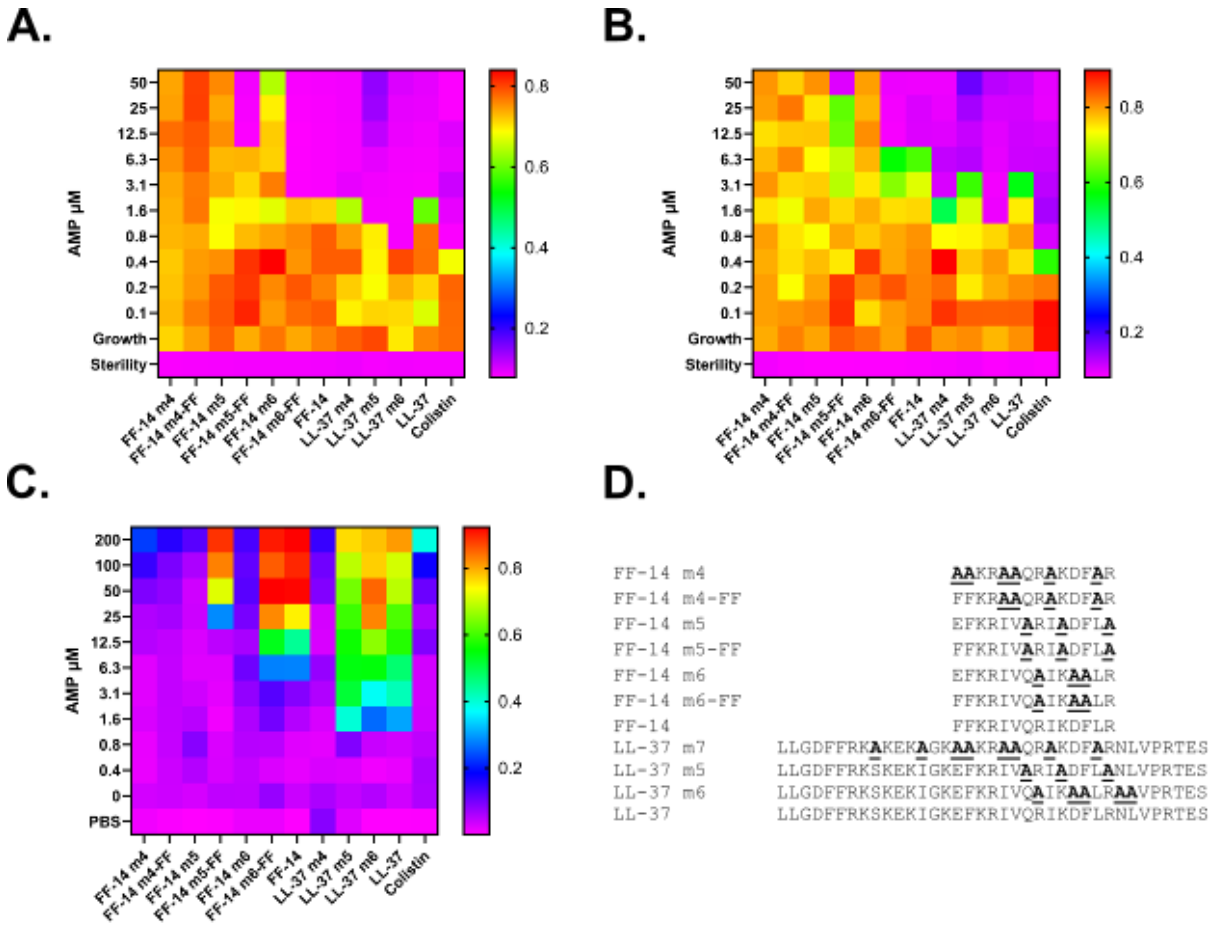
A.
B.
C.
D.
AMP µM
50
25
12.5
6.3
3.1
1.6
0.8
0.4
0.2
0.1
Growth
Sterility
200
100
0
PBS
0.8
0.6
0.4
0.2
FF-14 m4
FF-14 m4-FF
FF-14 m5
FF-14 m5-FF
FF-14 m6
FF-14 m6-FF
FF-14
LL-37 m4
LL-37 m5
LL-37 m6
LL-37
Colistin
FF-14 m4 AAKRAAQRAKDFAR
FF-14 m4-FF FFKRAAQRAKDFAR
FF-14 m5 EFKRIVARIADFLA
FF-14 m5-FF FFKRIVARIADFLA
FF-14 m6 EFKRIVQAIKAALR
FF-14 m6-FF FFKRIVQAIKAALR
FF-14 FFKRIVQRIKDFLR
LL-37 m7 LLGDFFRKAKEKAGKAAKRAAQRAKDFARNLVPRTES
LL-37 m5 LLGDFFRKSKEKIGKEFKRIVARIADFLANLVPRTES
LL-37 m6 LLGDFFRKSKEKIGKEFKRIVQAIKAALRAAVPRTES
LL-37 LLGDFFRKSKEKIGKEFKRIVQRIKDFLRNLVPRTES

Figure 1 – Antimicrobial and hemolytic activities of FF-14 derivatives correlate with each other. **A-B.** Antimicrobial susceptibility testing of *E. coli* (**A**) and *Pseudomonas* (**B**) was carried out using a series of grouped Ala mutants based on those previously used in full-length LL-37. Data show the raw OD600 after 18 hours of incubation at 37 °C; warm colors indicate bacterial growth, while cool colors are low / no growth. **C.** Hemolytic activity of each of the tested FF-14 derivatives as assessed by hemoglobin release after 18 hours of incubation at 37 °C. Cool colors indicate low signal at 414 nm, while warm colors are high signal; numbers are scaled to a 100% freeze-thaw hemolysis control. **D.** Sequence alignment showing each of the FF-14 mutants in **A-C** as well as the parent LL-37 mutants used as controls.

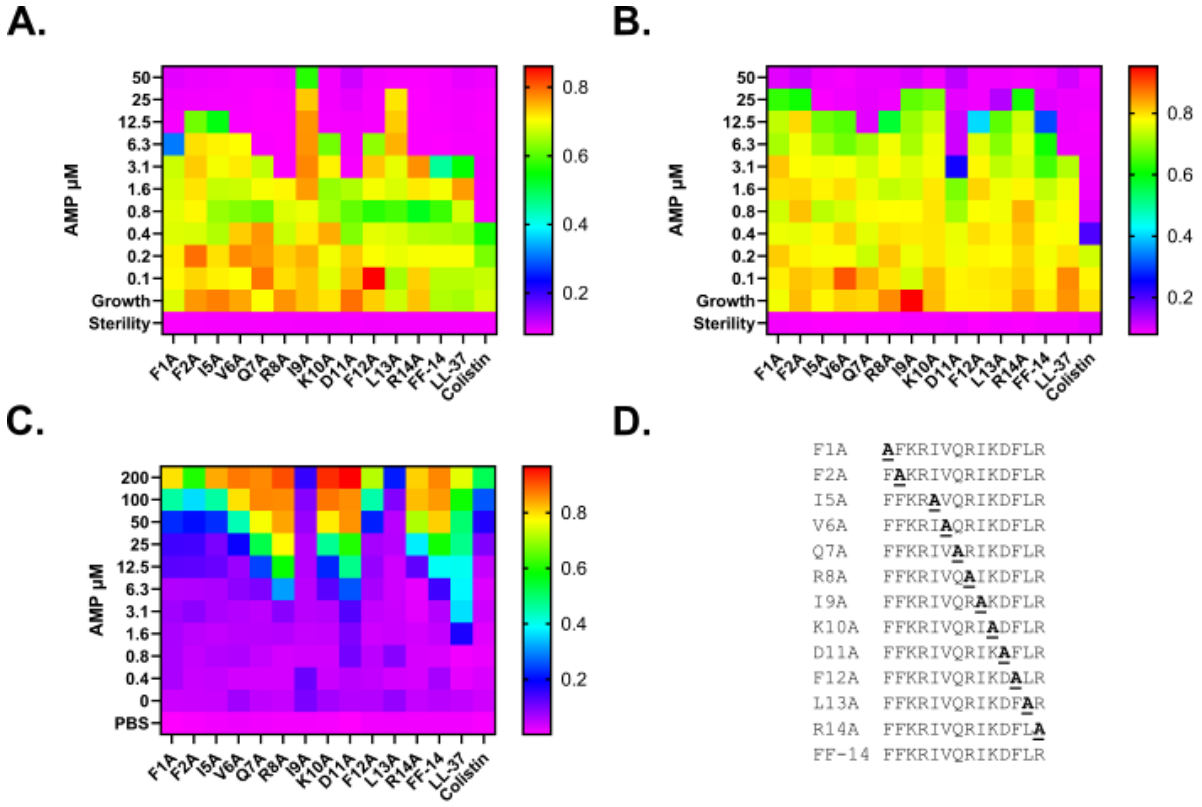
A.
B.
C.
D.
AMP µM
50
25
12.5
6.3
3.1
1.6
0.8
0.4
0.2
0.1
Growth
Sterility
200
100
0
PBS
F1A
F2A
I5A
V6A
Q7A
R8A
I9A
K10A
D11A
F12A
L13A
R14A
FF-14
LL-37
Colistin
0.8
0.6
0.4
0.2
F1A AFKRIVQRIKDFLR
F2A FAKRIVQRIKDFLR
I5A FFKRAVQRIKDFLR
V6A FFKRIAQRIKDFLR
Q7A FFKRIVARIKDFLR
R8A FFKRIVQAIKDFLR
I9A FFKRIVQRAKDFLR
K10A FFKRIVQRIADFLR
D11A FFKRIVQRIKAFLR
F12A FFKRIVQRIKDALR
L13A FFKRIVQRIKDFAR
R14A FFKRIVQRIKDFLA
FF-14 FFKRIVQRIKDFLR

Figure 2 – Antimicrobial and hemolytic activities of FF-14 single Ala mutants correlate with each other. A-B. Antimicrobial susceptibility testing of *E. coli* (**A**) and *Pseudomonas* (**B**) was carried out using a series of single Ala mutants in FF-14. Data show the raw OD600 after 18 hours of incubation at 37 °C; warm colors indicate high signal representing bacterial growth, while warm colors are low signal and growth. **C.** Hemolytic activity of each of the tested FF-14 derivatives as assessed by hemoglobin release after 18 hours of incubation at 37 °C. Cool colors indicate low signal at 414 nm, while warm colors are high signal; numbers are scaled to a 100% freeze-thaw hemolysis control. **D.** Sequence alignment showing each of the FF-14 mutants in **A-C**.

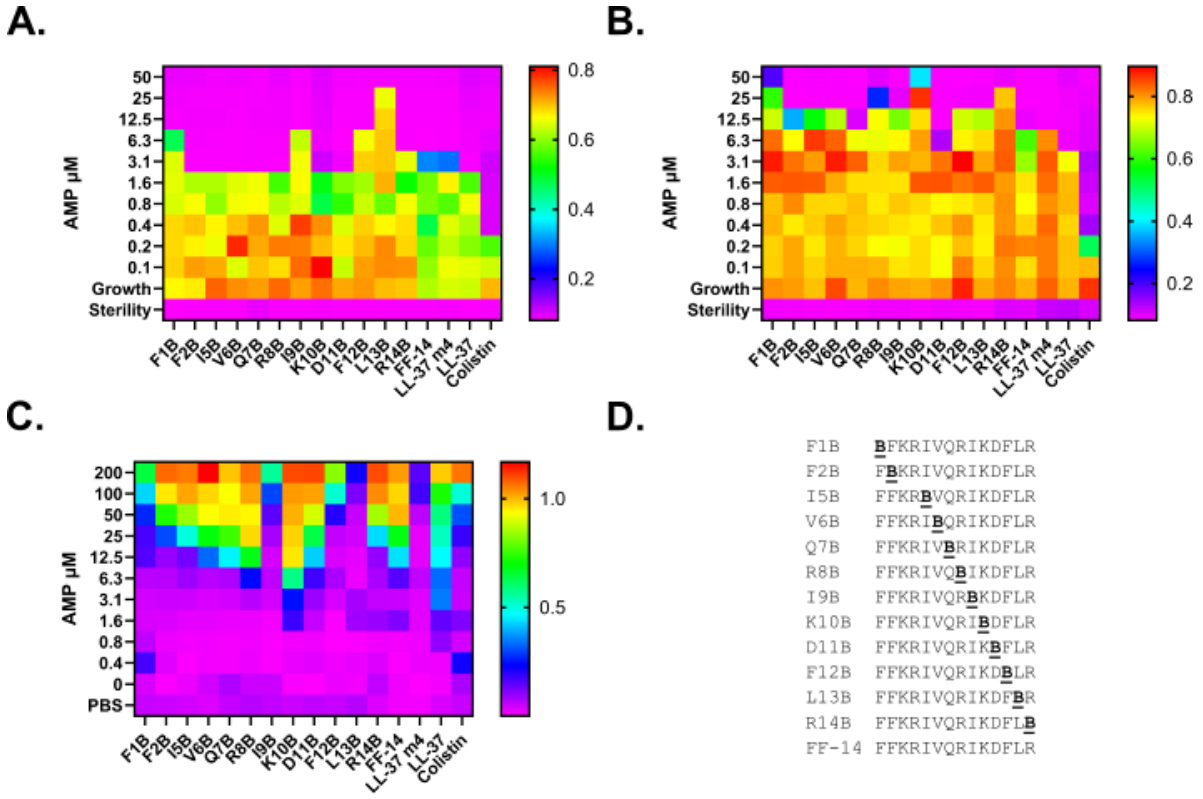
A.
B.
C.
D.
AMP µM
50
25
12.5
6.3
3.1
1.6
0.8
0.4
0.2
0.1
Growth
Sterility
200
100
0
PBS
F1B
F2B
I5B
V6B
Q7B
R8B
I9B
K10B
D11B
F12B
L13B
R14B
FF-14
LL-37 m4
LL-37
Colistin
0.8
0.6
0.4
0.2
1.0
0.5
F1B BFKRIVQRIKDFLR
F2B FBKRIVQRIKDFLR
I5B FFKRBVQRIKDFLR
V6B FFKRIBQRIKDFLR
Q7B FFKRIVBRIKDFLR
R8B FFKRIVQBIKDFLR
I9B FFKRIVQRBKDFLR
K10B FFKRIVQRIBDFLR
D11B FFKRIVQRIKBFLR
F12B FFKRIVQRIKDBLR
L13B FFKRIVQRIKDFBR
R14B FFKRIVQRIKDFLB
FF-14 FFKRIVQRIKDFLR

Figure 3 – Antimicrobial and hemolytic activities of Aib substitution mutants of FF-14. A-B. Antimicrobial susceptibility testing of *E. coli* (**A**) and *Pseudomonas* (**B**) was carried out using a series of single Aib mutants in FF-14. Data show the raw OD600 after 18 hours of incubation at 37 °C; warm colors indicate high signal representing bacterial growth, while warm colors are low signal and growth. **C.** Hemolytic activity of each of the tested FF-14 derivatives as assessed by hemoglobin release after 18 hours of incubation at 37 °C. Cool colors indicate low signal at 414 nm, while warm colors are high signal; numbers are scaled to a 100% freeze-thaw hemolysis control. **D.** Sequence alignment showing each of the FF-14 mutants in **A-C**.

A.

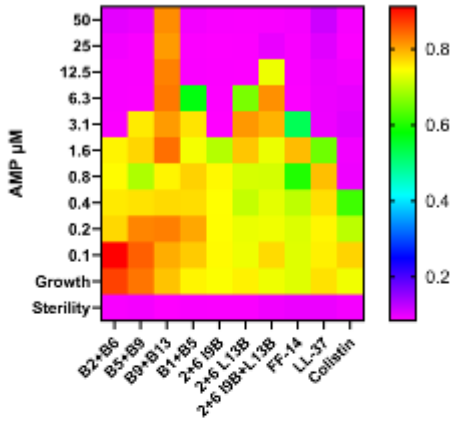

B.

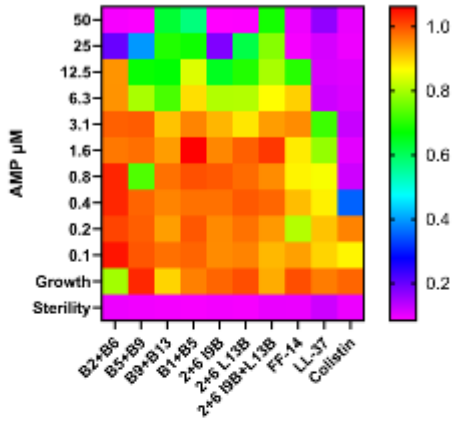

C.

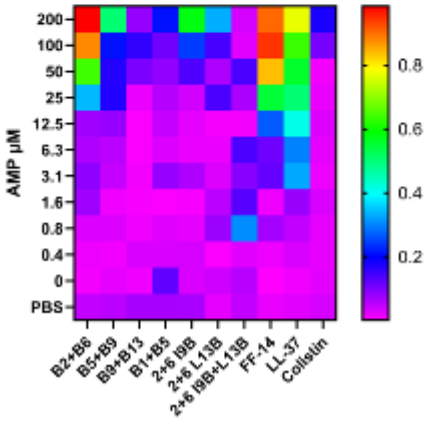

D.

F2B+V6B	F**B**KRI**B**QRIKDFLR
I5B+I9B	FFKR**B**VQR**B**KDFLR
I9B+L13B	FFKRIVQR**B**KDF**B**R
F1B+I5B	**B**FKR**B**VQRIKDFLR
2+6 I9B	F**B**KRI**B**QR**B**KDFLR
2+6 L13B	F**B**KRI**B**QRIKDF**B**R
2+6 I9B+L13B	F**B**KRI**B**QR**B**KDF**B**R
FF-14	FFKRIVQRIKDFLR

Figure 4 – Antimicrobial and hemolytic activities of multiple Aib substitution mutants of FF-14. **A-B.** Antimicrobial susceptibility testing of *E. coli* (**A**) and *Pseudomonas* (**B**) was carried out using a series of single 2-4 Aib mutations in FF-14. Data show the raw OD600 after 18 hours of incubation at 37 °C; warm colors indicate higher bacterial growth, while warm colors are low / no growth. **C.** Hemolytic activity of each of the tested FF-14 derivatives as assessed by hemoglobin release after 18 hours of incubation at 37 °C. Cool colors indicate low signal at 414 nm, while warm colors are high signal; numbers are scaled to a 100% freeze-thaw hemolysis control. **D.** Sequence alignment showing each of the FF-14 Aib mutants in **A-C**.

A.

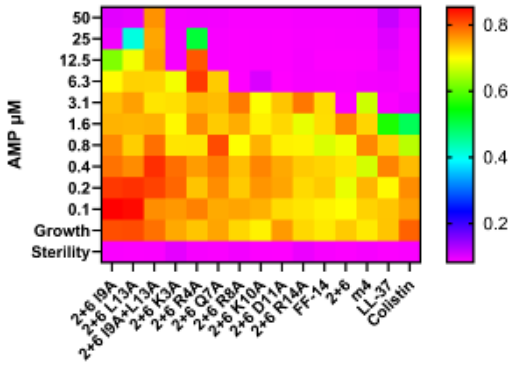

B.

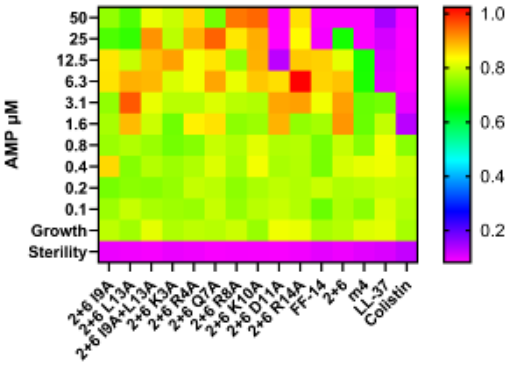

C.

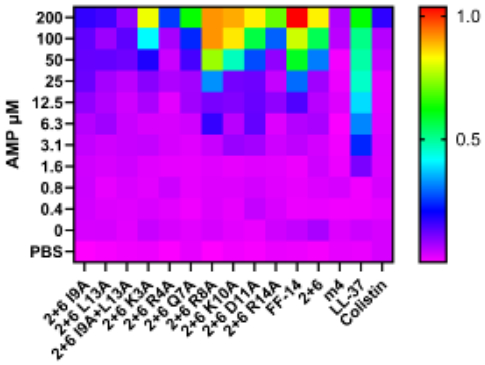

D.

2+6 I9A	FBKRIBQR**A**KDFLR
2+6 L13A	FBKRIBQRIKDF**A**R
2+6 I9A+L13A	FBKRIBQR**A**KDF**A**R
2+6 K3A	FB**A**RIBQRIKDFLR
2+6 R4A	FBK**A**IBQRIKDFLR
2+6 Q7A	FBKRIB**A**RIKDFLR
2+6 R8A	FBKRIBQ**A**IKDFLR
2+6 K10A	FBKRIBQRI**A**DFLR
2+6 D11A	FBKRIBQRIK**A**FLR
2+6 R14A	FBKRIBQRIKDFL**A**
FF-14	FFKRIVQRIKDFLR

Figure 5 – Antimicrobial and hemolytic activities of Ala mutants in an F2B+V6B background. **A-B.** Antimicrobial susceptibility testing of *E. coli* (**A**) and *Pseudomonas* (**B**) was carried out using a series of single Ala mutations in FF-14 F2B+V6B. Data show the raw OD600 after 18 hours of incubation at 37 °C; warm colors indicate high signal representing bacterial growth, while warm colors are low signal and growth. **C.** Hemolytic activity of each of the tested FF-14 derivatives as assessed by hemoglobin release after 18 hours of incubation at 37 °C. Cool colors indicate low signal at 414 nm, while warm colors are high signal; numbers are scaled to a 100% freeze-thaw hemolysis control. **D.** Sequence alignment showing each of the mutants in **A-C**.

	% Helix at 37 °C			MIC			20% Hemolysis			Fold MIC / Hemolysis		
	Ala	**Aib**	**Fold Δ B:A**	**Ala**	**Aib**	**Fold Δ A:B**	**Ala**	**Aib**	**Fold Δ B:A**	**Ala**	**Aib**	**Fold Δ B:A**
F1	39.6	51.7	1.3	12.5	12.5	1.0	25	25	1.0	2.0	2.0	1.0
F2	16.7	74.2	4.4	25	3.1	8.1	25	12.5	0.5	1.0	4.0	4.0
I5	55.3	91.6	1.7	25	3.1	8.1	25	12.5	0.5	1.0	4.0	4.0
V6	18.7	100	5.3	12.5	3.1	4.0	25	6.3	0.3	2.0	2.0	1.0
Q7	26.5	96.5	3.6	6.3	3.1	2.0	6.3	6.3	1.0	1.0	2.0	2.0
R8	100	100	1.0	3.1	3.1	1.0	6.3	3.1	0.5	2.0	1.0	0.5
I9	8.1	54	6.7	100	12.5	8.0	200	50	0.3	2.0	4.0	2.0
K10	16.2	90.3	5.6	12.5	3.1	4.0	6.3	1.6	0.3	0.5	0.5	1.0
D11	92.7	68.7	0.7	3.1	3.1	1.0	3.1	6.3	2.0	1.0	2.0	2.0
F12	75.9	84.7	1.1	12.5	12.5	1.0	50	25	0.5	4.0	2.0	0.5
L13	10.3	18.2	1.8	50	50	1.0	200	100	0.5	4.0	2.0	0.5
R14	16	74.1	4.6	6.3	6.3	1.0	12.5	12.5	1.0	2.0	2.0	1.0
		Avg Δ	3.2		Avg Δ	3.4		Avg Δ	0.7		Avg Δ	1.6

Table 1 – Effect of Aib on FF-14 helical content and activities. Table 1 summarizes the quantitative effects of replacing a given residue in FF-14 with Aib in place of Ala. % Helix at 37 °C shows the percentage of helical content in each peptide as calculated by BeStSel based on the spectra shown in **Supplementary Figures 58** and **92**, with fold-changed derived by dividing the Aib percentage by the Ala percentage. MIC indicates the minimum inhibitory concentrations of each peptide against *E. coli* as shown in **Figures 2** and **4** and associated **Supplementary Figures**, with the fold change derived by dividing the Ala MIC by the Aib MIC, such that larger numbers indicate more potent antimicrobial activity. 20% Hemolysis indicates the highest peptide concentration with less than 20% hemolysis as shown in **Figures 2** and **4** and associated **Supplementary Figures**, with the fold change derived by dividing the Aib concentration by the Ala concentration, such that larger numbers indicate less toxic activity in Aib-containing derivatives. Fold MIC / Hemolysis indicates the ratio of the 20% Hemolysis threshold for each peptide divided by the MIC for each peptide against *E. coli*. The fold change is derived by dividing the Aib ratio by the Ala ratio, such that larger numbers indicate improved *in vitro* therapeutic indices.